

Structure-Dependent Charge Transfer in Molecular Perylene-Based Donor/Acceptor Systems and Role of Side Chains

Valentina Belova,* Alexander Hinderhofer,* Clemens Zeiser, Timo Storzer, Jakub Rozbořil, Jan Hagenlocher, Jiří Novák, Alexander Gerlach, Reinhard Scholz, and Frank Schreiber

Cite This: *J. Phys. Chem. C* 2020, 124, 11639–11651

Read Online

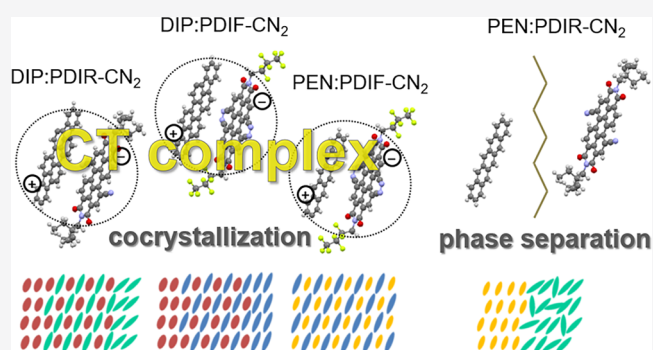
ACCESS |

Metrics & More

Article Recommendations

Supporting Information

ABSTRACT: In organic electronics and optoelectronics several crucial physical processes are related to charge transfer (CT) effects. In this work, we investigate mixing behavior and intermolecular coupling of donor and acceptor molecules in thin films prepared by organic molecular beam deposition (OMBD). Diindenoperylene (DIP) and pentacene (PEN) are used as the donor materials, and perylene diimide derivatives PDIR-CN₂ and PDIF-CN₂ as the acceptor materials. The formation of charge transfer complexes coupled in the electronic excited state vs. noninteracting phase separating components is studied by structural and optical techniques. The CT mechanism and properties are considered in close connection with the thin film microstructure of the D/A blends which can be controlled via a change of the molecule geometry and/or growth temperature. We discuss two key findings for our systems: (1) The CT intensity correlates directly with the possibility of cocrystallization between acceptor and donor. (2) Side chain modification to tune the ground state energy levels has nearly no effect on the energy of the excited state CT, whereas replacement of molecular core modifies the CT energy correspondingly.



INTRODUCTION

Charge transfer (CT) between a donor (D) and an acceptor (A) is a crucial phenomenon for performance of organic photovoltaic (OPV) devices.^{1–4} Since this complex process mediates creation of charge carriers at a D/A interface, and their potential subsequent recombination, its mechanism needs to be understood. Over the past years the most established practical solutions in the field of OPVs were based on polymer/fullerene (or derivatives) combinations.^{5–11} However, despite reaching efficiencies of over 10%, fullerene-based solar cells meet a number of limitations, which might be overcome by small molecule semiconductors.^{12–17} Small molecule semiconductors provide almost countless possibilities for the tailoring of device properties.^{18–20} For example, by choosing different organic compounds, the resulting energy gap (E_{DA}) between a donor ionization energy (IE) and an acceptor electron affinity (EA) can be tuned. Thus, (i) a larger E_{DA} results in a higher open circuit voltage (V_{OC})²¹ and smaller nonradiative energy losses (in the absence of any influence of the morphology).²² (ii) In the case of a narrower E_{DA} , a direct excitation of low-lying CT states leads to broadening of the optical absorption wavelength range in the near-infrared region most favorable for solar energy harvesting. However, the CT states might also serve as efficient recombination channels for excitons.^{23–28} This aspect is particularly important and has to

be taken into consideration when designing an active layer in a bulk heterojunction (BHJ) configuration. Compared with planar heterojunctions, the BHJ configuration provides a larger interface area between donor and acceptor and would therefore be more advantageous in terms of photon to charge carrier quantum yield.

Consequently, for BHJs the morphology of the mixed layer plays a paramount role.^{4,29–31} First of all, charge transport suffers from numerous in-gap trap states introduced by lattice disorder.³² Another factor is the nucleation of one of the pure phases, in particular an acceptor phase, along with the presence of a mixed phase which is considered as a beneficial condition for increasing charge separation rates.^{33,34} A higher dielectric constant of the acceptor phase is required to lower the Coulomb exciton binding energy and facilitate exciton dissociation.³⁵ Furthermore, crystalline domains of pure phases provide percolation pathways for delivering charge carriers to the electrodes.³⁶ The exciton diffusion length in polycrystalline

Received: January 10, 2020

Revised: April 28, 2020

Published: April 29, 2020



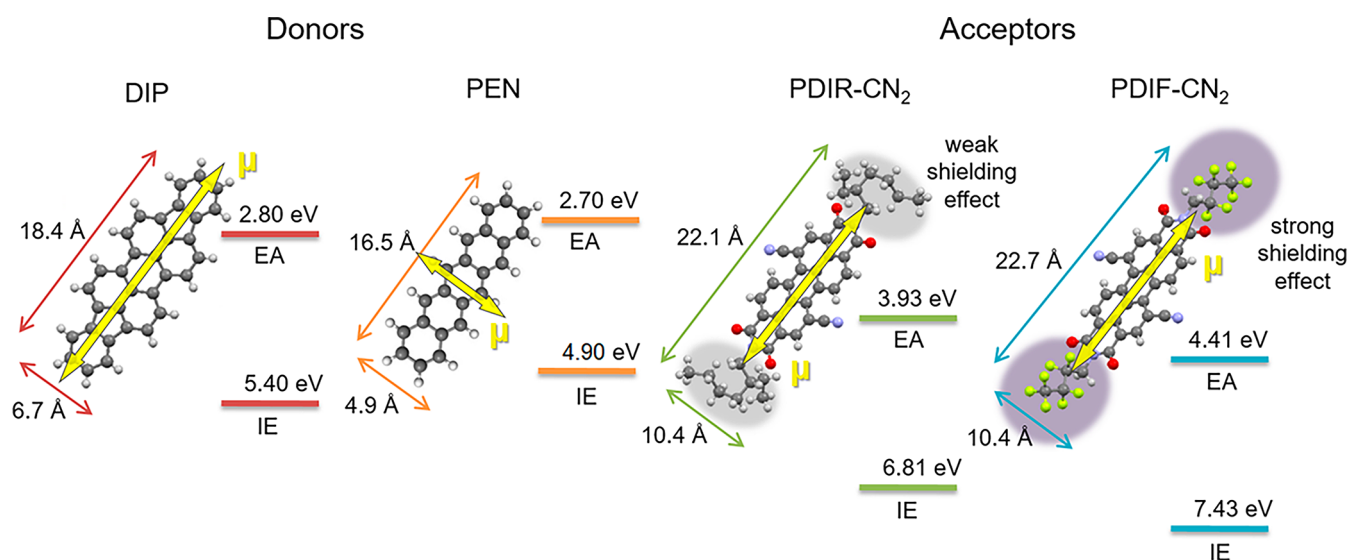


Figure 1. Small molecule organic semiconductors employed in the study. Atom color code is the following: C, dark gray; H, light gray; O, red; N, purple; F, green. Molecule dimensions and energy levels are relevant for the crystal packings. Yellow arrows depict the orientation and relative size of the dipole moment μ of the transition between the first highest occupied and lowest unoccupied molecular orbitals (HOMO and LUMO, respectively). Dark regions around the acceptors' side chains illustrate their steric shielding effect. The IE and EA levels for thin films are taken from refs 48 and 55–57.

organic semiconductor films can also be controlled by the grain size through minimization of exciton trapping at grain boundaries.^{37,38} Thus, processes of intermixing, phase separation, crystallization in binary molecular mixtures of donor and acceptor species, as well as the correlation with formation of CT complexes require detailed investigation.

Previous studies^{39–41} carried out in this context considered aspects of sterical compatibility in two-phase mixed systems, where the dominating factors for phase separation are differences in geometry and shape of the respective components (e.g., fullerenes mixed with rod-like molecules or planar shaped molecules). Even a deviation of the conjugated core length or an alternating aromatic ring fusion can induce nucleation of the pure phases, since the internal molecular degrees of freedom are one of the molecular packing guides.⁴² However, when donor and acceptor species are mixed, an additional electrostatic attraction component can play the role of a stabilizing force for the cocrystal.^{43–45} The competition of different kinds of intermolecular interactions is therefore of great interest for the systematic understanding of D/A blends.

In this work, we present a study of the mixing behavior and structure-dependent CT in different small-molecule D/A systems. As acceptor materials, two perylene diimide derivatives (PDIs) were chosen: *N,N'*-bis(2-ethylhexyl)-dicyanoperylene-3,4:9,10-bis(dicarboximide) (PDIR-CN₂ or PDIR)⁴⁶ and *N,N'*-1*H*,1*H*-perfluorobutylidicyanoperylene-3,4:9,10-bis(dicarboximide) (PDIF-CN₂ or PDIF)⁴⁷ containing alkyl and fluoroalkyl chain substituents at an imide position (Figure 1). It was shown that the side chains contribute to a steric shielding effect of the intermolecular interaction between the perylene diimide backbones, hindering crystallization during thin film deposition.⁴⁸ The effect is significantly stronger in the case of the fluorinated chains, leading to very limited crystal quality in PDIF-CN₂ films grown at room substrate temperature (RT). Thus, by use of these compounds, the influence of variable intermolecular coupling on a possible mixing behavior can be probed in such systems. Because of the

partial fluorination the EA level of PDIF-CN₂ in thin films is shifted down by ~ 0.5 eV compared with PDIR-CN₂ as detected by ultraviolet photoelectron spectroscopy (UPS),⁴⁸ the frontier molecular orbitals seem to be barely affected, since they are distributed over the perylene backbone.⁴⁹

As donor materials, two archetypal p-type small-molecule semiconductors were chosen: diindenoperylene (DIP, C₃₂H₁₆) and pentacene (PEN, C₂₂H₁₄) (Figure 1). Both compounds are known for their applications in organic electronics, in particular, as donors in OPV devices^{50–52} and p-type semiconductors in organic field-effect transistors (OFETs).^{53,54} DIP has a molecular structure based on a perylene core similar to the PDIs but does not contain bulky side groups, which makes it a sterically favorable match for both acceptors. In contrast, due to the smaller size of PEN, we observe different interaction scenarios upon mixing with PDIs. The energy gap in PEN thin films is smaller than in DIP, and the IE is lower by ~ 0.5 eV (Figure 1).^{55–57} Thereby, the variation of both donors and acceptors covers four different options for tuning the E_{DA} .

The results are organized as follows. First, a structural study of intermixing and cocrystal formation vs phase-separation in coevaporated D/A thin films performed by X-ray diffraction (XRD) is given in the “Structure Analysis” subsection complemented by a brief morphological description in “Surface Morphology”. The second part of the results, “Optical Spectroscopy”, is devoted to an analysis of intermolecular coupling between D and A molecules in thin film blends by Fourier Transform Infrared (FTIR) spectroscopy and optical absorption and emission spectroscopy for the characterization in the ground and excited electronic states, respectively. In “Discussion” we correlate results from both structural and optical parts based on the role of intermolecular binding energies.

EXPERIMENTAL METHODS

Thin films were produced by organic molecular beam deposition (OMBD) in ultrahigh vacuum (UHV) chambers

on silicon wafers covered by a native SiO_x layer at a base pressure of 1×10^{-9} mbar (stationary chamber) and 1×10^{-8} mbar (portable chamber) and a substrate temperature T_{sub} of 70 and 140 °C. Binary mixed films were prepared by coevaporation with an average total rate of 0.2 nm/min. The uncertainty for the mixing ratios is about $\pm 10\%$. Organic semiconductor materials were purchased from Polyera, U.S.A. (PDIR-CN₂ and PDIF-CN₂), Prof. Pflaum, Germany (DIP), and Sigma-Aldrich, Germany (PEN).

XRD real-time and postgrowth characterization was performed at the European Synchrotron Radiation Facility (France) and at the Soleil Synchrotron (France). A beam energy of 14 keV was applied.

Optical absorption spectra were evaluated from data acquired by variable angle spectroscopic ellipsometry (VASE) using a Woollam M2000 ellipsometer (LOT-QuantumDesign GmbH, Germany).^{58,59} Photoluminescence spectra were recorded with a Labram HR 800 spectrometer (Horiba Jobin Yvon, France) containing a CCD-1024×256-OPEN-3S9 detector and a frequency-doubled Nd:YAG laser (532 nm wavelength).⁶⁰ Changes in optical absorption spectra were monitored during film growth using a differential reflectance spectroscopy (DRS) setup consisting of a fiber coupled USB2000+ spectrometer and a DH-2000 lamp (Ocean Optics, The Netherlands).⁶¹ Atomic force microscopy (AFM) images were taken with a JPK NanoWizard II setup (JPK Instruments AG, Germany) in tapping mode.⁶² Infrared spectra were acquired using a Vertex 70 (Bruker, Germany) spectrometer in transmission mode at 74° (Brewster's angle of silicon).

RESULTS AND DISCUSSION

Structure Analysis. Organic small molecule semiconductor thin films prepared by vacuum deposition on polycrystalline substrates typically exhibit uniaxial polycrystallinity, i.e., can be considered as a “two-dimensional powder”, keeping a preferential orientation along the surface normal (out-of-plane direction).⁶³ Reciprocal space maps of binary equimolar (mixing ratio 1:1) mixed thin films of DIP:PDIR-CN₂ as well as DIP:PDIF-CN₂ are shown in Figure 2a,b. Other mixing ratios (3:1 and 1:2) are provided in the Supporting Information, Figure S1. A growth temperature of 140 °C was chosen as a temperature at which both acceptor compounds display the highest crystallinity. PDIR-CN₂ exhibits coexistence of two polymorphs.⁴⁸ In contrast, the DIP crystalline structure does not undergo significant changes when going from room temperature (30 °C) to the high substrate temperature (HT).⁶⁴ In both equimolar mixtures the formation of mixed phases is clearly observed. The calculated lattice parameters are given in Table 1. The mixed phase unit cell volume is consistent with a sum of the donor and acceptor unit cells. For nonequimolar mixtures, nucleation of a pure phase of the excess component occurs (Supporting Information, Figure S1) at HT. Indexing of the respective phases reflections indicate that the *c* axes, and therefore also the molecular axes, are nearly parallel to the sample surface normal for the cocrystal phases. The same unit cell orientation was noticed for all cocrystals reported in this paper whenever uniaxial texturing appeared. The observed tip-on molecular orientation is typical for growth of rod-like molecules on SiO_x and weakly interacting substrates in general.

The diffraction pattern of DIP:PDIF-CN₂ 1:2 (Supporting Information, Figure S1d) does not correspond to the crystal

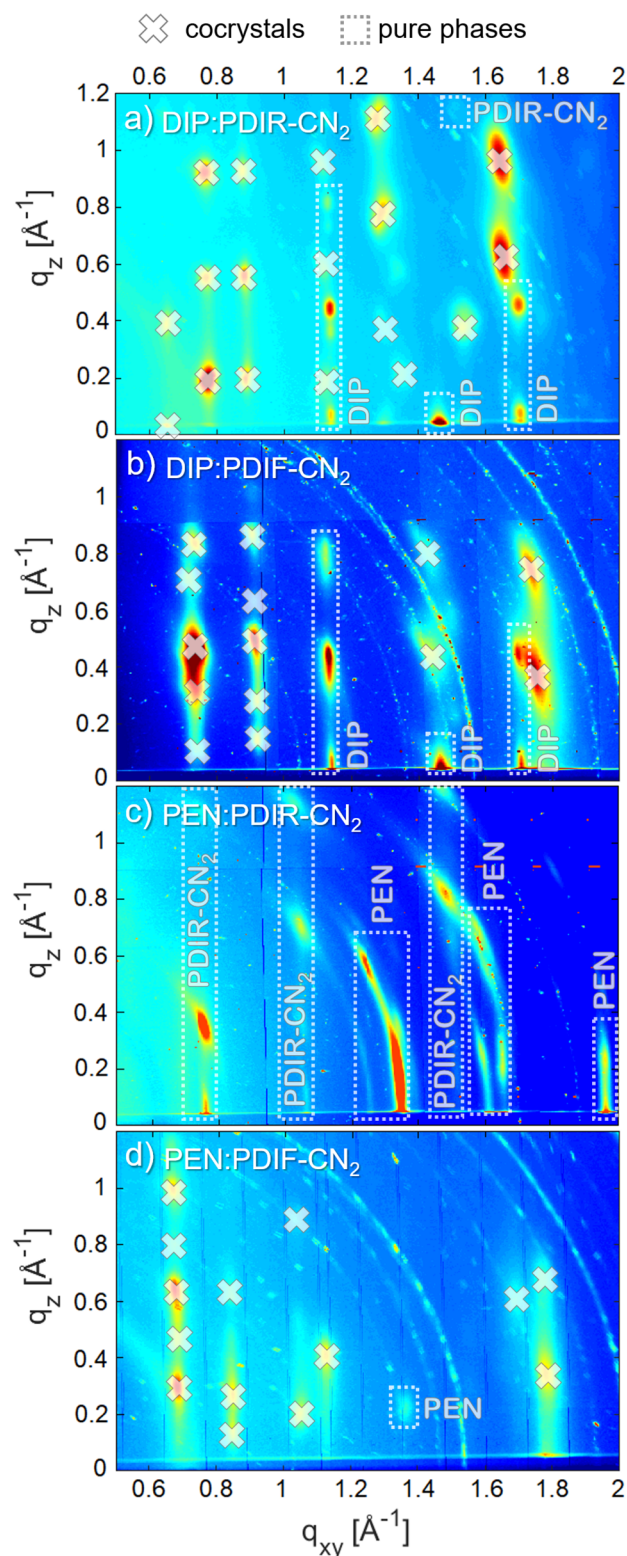


Figure 2. Reciprocal space maps of equimolar (1:1) DIP:PDIR-CN₂ (a) and DIP:PDIF-CN₂ (b) films deposited at 140 °C and PEN:PDIR-CN₂ (c) and PEN:PDIF-CN₂ (d) films deposited at 70 °C. The *z*-axis is perpendicular to the substrate surface (*xy* plane). The crosses in (a), (b), and (d) indicate the reflection pattern from the crystalline 1:1 mixed phases (aligned with the peak intensity maxima). Areas with peaks of the pure donor and acceptor phases are highlighted with the dotted rectangles and labeled correspondingly. No mixed phase is observed in PEN:PDIR-CN₂ (c). Note that both bulk and thin film phases of PEN are present in (c).

Table 1. Unit Cell Parameters and Volumes of Pure Compounds and of the Identified Cocrystal Phases

D/A system	<i>a</i> , Å	<i>b</i> , Å	<i>c</i> , Å	α , deg	β , deg	γ , deg	<i>V</i> , Å ³	<i>Z</i> ^a
DIP (HT phase) ⁶⁵	7.17	8.55	16.80	90	92.42	90	1029	2
PEN (tf ^b) ⁶⁶	5.92	7.54	15.63	81.5	87.2	89.9	689	2
PEN (bulk) ⁶⁷	6.06	7.90	15.01	81.6	77.2	85.8	692	2
PDIR-CN ₂ (RT phase) ⁴⁸	6.44	8.99	16.59	87.52	86.2	112.6	883	1
PDIR-CN ₂ (HT phase) ⁴⁸	9.33	12.07	16.93	105.2	90	90	1839	2
PDIF-CN ₂ (at HT) ⁴⁸	5.53	7.52	20.4	87.12	101.5	106.3	798	1
DIP:PDIR-CN ₂ 1:1	8.45	10.07	17.41	86.09	103.9	103.6	1396	2
DIP:PDIF-CN ₂ 1:1	8.72	8.97	17.25	85.83	97.9	101.9	1307	2
DIP:PDIF-CN ₂ 1:2	8.49	11.01	18.08	86.72	97.9	109.9	1573	2
PEN:PDIF-CN ₂ 1:1	7.44	9.30	17.95	96.55	81.7	94.3	1218	2

^a*Z*: number of molecules per unit cell. ^btf: thin film.

structure of PDIF-CN₂ observed in the pristine films. Interestingly, the calculated volume of the possible unit cell is almost twice the original one (1573 Å³ vs 798 Å³). This might be a hint for another polymorph similar to the HT-phase of PDIR-CN₂ containing two molecules per unit cell. For a detailed understanding of the influence of DIP on PDIF-CN₂ growth, nonequimolar coevaporated blends and consecutively deposited heterostructures have to be closely investigated.

In addition, we note that at RT, where both acceptor materials exhibit a less ordered structure, only short-range order is present in the mixed films as shown in the Supporting Information in Figure S2. One can observe the presence of the distorted pure phases in DIP:PDIR-CN₂ series which is not the case for DIP:PDIF-CN₂.

Diffraction images of mixtures with PEN deposited at 70 °C are shown in Figure 2c,d. The lower temperature is chosen due to weak adsorption of PEN molecules on SiO_x. At this temperature neither PDIR-CN₂ nor PDIF-CN₂ undergoes a phase transition and has structural properties similar to those at RT.⁴⁸ PDIR-CN₂ thin films contain crystalline domains of the RT-polymorph, and PDIF-CN₂ thin films exhibit a broad scattering feature from the nearly amorphous structure. Both components PEN and PDIR-CN₂ maintain their respective diffraction patterns in the mixed film, and no further diffraction peaks are observed. This indicates a strong phase separation between the species with their unit cell remaining unperturbed. In contrast, formation of a pronounced cocrystal is observed for PEN:PDIF-CN₂ mixed films (Figure 2d and Supporting Information, Figure S3), in which the excess of PEN molecules nucleates separately (Supporting Information, Figure S3a) and the excess of the amorphous PDIF-CN₂ phase leads to a “dilution” of the mixed phase: the crystalline order decreases in the amorphous matrix (Supporting Information, Figure S3c,d).

As a short summary of this subsection, we point out that formation of the ordered mixed phases is clearly evidenced in both DIP systems and in PEN blended with PDIF-CN₂ whereas PEN:PDIR-CN₂ is the only system showing a tendency toward phase separation. We also note that, for all crystalline mixed phases, molecules are oriented “up-right” with the long molecular axis almost parallel to the sample surface normal (Table 1).

Surface Morphology. The shape of the D/A cocrystals can be considered in more detail now in terms of surface morphology. AFM images of the pure films and equimolar blends are provided in Figure 3. Both pure DIP and PDIR-CN₂ at HT follow the layer-plus-island growth (Stranski–Krastanov) mode forming flat terraces on top of the previous layer. As can be seen from the round shape of the terraces,

there is no favored growth direction within the surface plane. PDIF-CN₂ at HT reveals growth along all three axes. Thus, roundish islands dominate on the surface. Yet upon intermixing of PDIs with DIP at HT, pronounced needle-like features emerge. The islands are longer in DIP:PDIR-CN₂, 0.5–0.8 μm as opposed to 0.2–0.5 μm in DIP:PDIF-CN₂. This indicates a preferred one-dimensional (1D) packing that most probably occurs along the direction of the π–π stacking between the D and A moieties.^{68,69} PEN molecules are arranged into so-called “wedding-cake” islands, a morphology typical of rod-like organic molecules. The equimolar blend with PDIR-CN₂ features a surface consisting of round domains with a diameter of 0.1–0.5 μm. The mixture with PDIF-CN₂ exhibits small elongated grains with a lateral size of 0.05–0.3 μm which might be related to the 1:1 cocrystal.

Optical Spectroscopy. FTIR Measurements. In order to test a possible ground-state CT, FTIR measurements were performed. The recorded transmission spectra are presented in Figure 4. The characteristic shift of the –CN vibrational stretching mode can be used to estimate the degree of partial CT. By assuming a linear shift between the neutral and the ionized molecule, we find in DIP:PDIF-CN₂ and PEN:PDIF-CN₂ a shift similar to that in DIP:PDIR-CN₂, which was previously assigned to a partial CT of about 0.2 e in the ground state.^{57,70,71} Noteworthy, all three systems exhibit roughly the same shift of 4–5 cm^{–1}. At the same time, no distinct shift in the PEN:PDIR-CN₂ spectrum is observed. This matches exactly the mixing behavior observed by means of XRD as discussed in the previous section. A similar correlation between vibrational-mode shifts and D/A mixing/demixing has been observed for polymer:fullerene systems.⁷² This observation confirms that the formation of a mixed cocrystal coincides with a partial CT in the ground state, whereas phase separating material combinations do not exhibit any detectable ground state CT.

Absorption Spectroscopy. In general, a modification of the environment is reflected in the molecular electronic structure through new features (e.g., energy shifts, band shape modification, appearance/disappearance of new transitions) in the optical absorption and emission spectra. Thus, the first fundamental transitions around 2.2 eV in optical absorption spectra in Figure 5a,b of pristine PDIR-CN₂ and PDIF-CN₂ grown at HT originate from *J*-like coupling due to a longitudinal displacement between molecules in the crystal phases.⁴⁸ The absorption spectrum of DIP also undergoes changes in comparison with the solution spectrum due to the long-range intermolecular interactions upon crystallization in thin films.^{61,73} It is worth mentioning that in solution both DIP

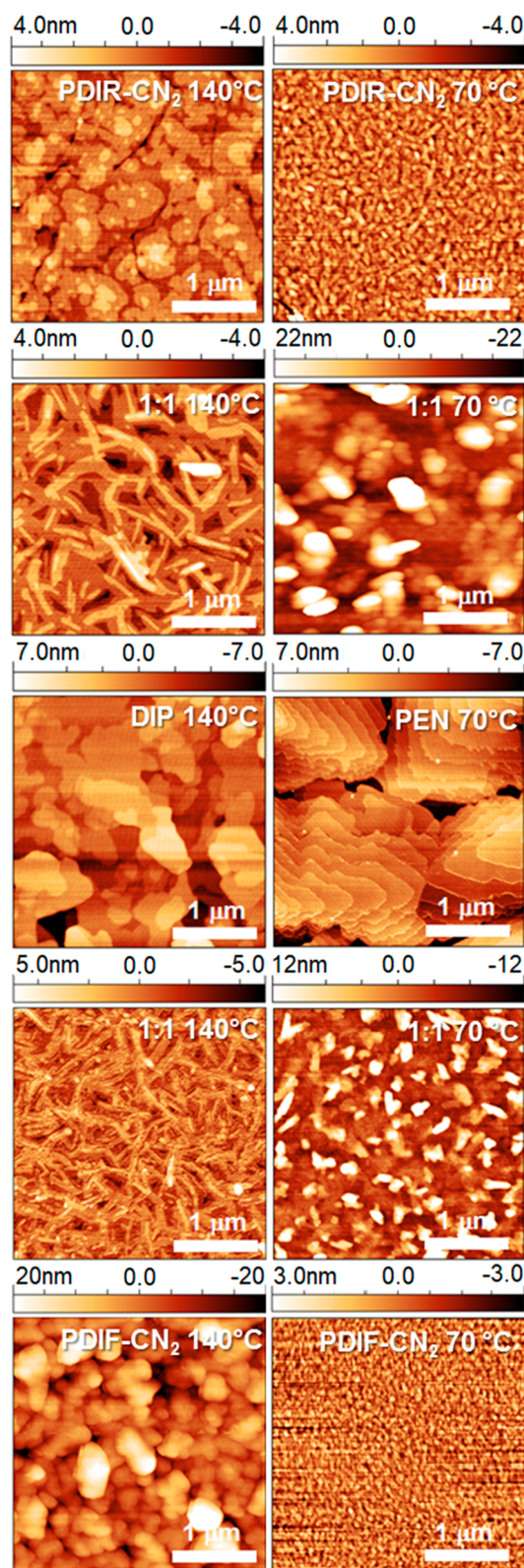


Figure 3. AFM images, $3 \mu\text{m} \times 3 \mu\text{m}$, of pristine and 1:1 films: left column, DIP systems (grown at 140°C); right column, PEN systems (grown at 70°C).

and PDI exhibit a similar absorption spectrum with the first transition of around 2.35 eV. For PEN, the optical energy gap in solution is smaller (2.1 eV).⁷⁴ Upon formation of a D/A cocrystal the resulting absorption spectrum of thin films with a

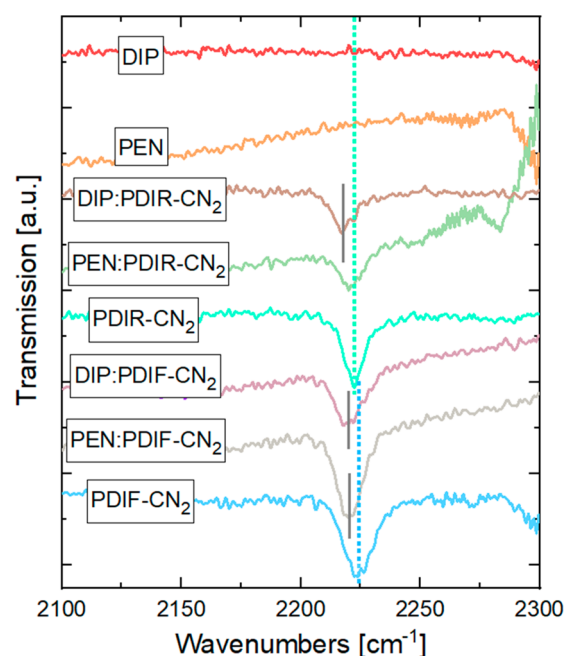


Figure 4. FTIR transmission spectra of pristine DIP, PEN, PDIR-CN₂, PDIF-CN₂, and mixed films (1:1). A shift of the characteristic -CN₂ stretching mode at 2222.3 cm^{-1} for PDIR-CN₂ (light green) and 2224.1 cm^{-1} for PDIF-CN₂ (blue) serves as an indication of a partial CT in the ground state.⁵⁷ The data are offset for clarity.

mixing ratio close to equimolar resembles neither spectra of the individual molecules nor spectra of the pristine thin films, as it is the case for DIP:PDIR-CN₂, DIP:PDIF-CN₂, and PEN:PDIF-CN₂ (Figure 5a,b,d). Intermolecular coupling favored by the closely packed D/A molecules in the mixed phases causes changes in the band shape and appearance of new absorption bands in the subgap energy regions (see insets in Figure 5). Such subgap absorption bands are generally attributed to a direct CT transition from the HOMO of a donor molecule (HOMO_D) to the LUMO of an acceptor molecule (LUMO_A) upon excitation.^{5,57,75,76} The spectra of the equimolar blends in both DIP systems look similar to a relatively strong complex CT band between 1.4 and 2.1 eV, and the intensity center of mass shifted toward higher energy (2.5 eV). The similarity can be explained by DIP molecules interacting directly with the perylene diimide backbones, which are identical for both PDIR-CN₂ and PDIF-CN₂, whereas the acceptors' optical properties in thin films are affected by the environment via the different side chains.⁴⁸ If the mixing ratio deviates from 1:1, optical traits inherent to the pure donor or acceptor crystalline phases become more pronounced, making the resulting spectrum a superposition of the pure materials and the mixed phase. This observation supports the conclusions on the structure made in the previous subsection.

In the PEN:PDIR-CN₂ system, where strong phase separation is observed, the optical behavior is different (Figure 5c). Spectra of the mixed films resemble a simple superposition of both original components with the contributions proportional to the $\epsilon_{2,xy}$ of the pristine films and gradually changing according to the mixing ratio. In this, the optical features attributed to the pristine crystal phases, such as a Davydov splitting of the red-shifted 0–0 transition between 1.8 and 2.0 eV in PEN and the red-shifted 0–0 transition in PDIR-CN₂ at around 2.2 eV, persist in the blends. Note that the oscillator

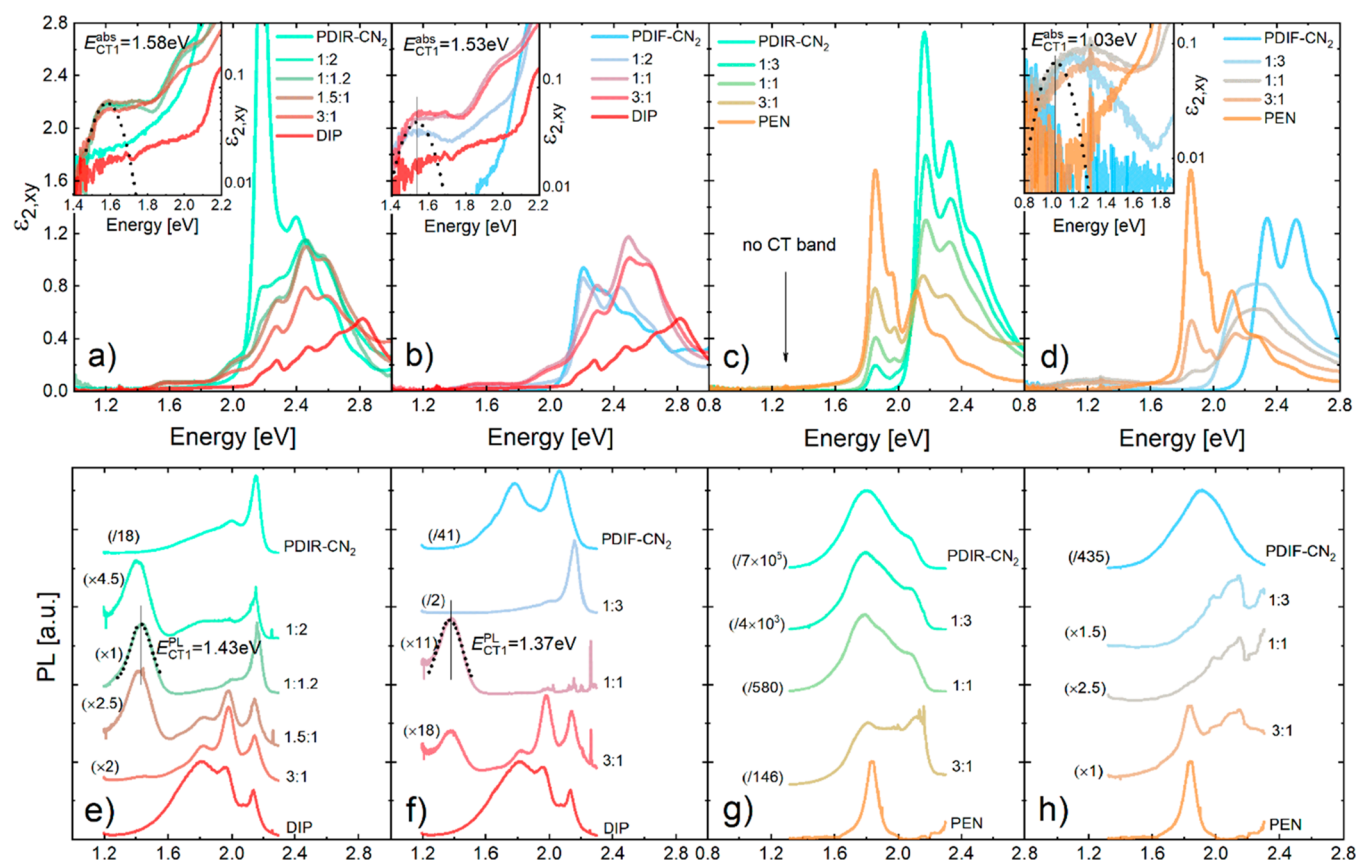


Figure 5. (a–d) Optical absorption spectra in the in-plane direction evaluated from ellipsometry data and (e–h) photoluminescence spectra recorded at 20 °C: (a, e) DIP:PDIR-CN₂ at 140 °C; (b, f) DIP:PDIF-CN₂ at 140 °C; (c, g) PEN:PDIR-CN₂ at 70 °C; (d, h) PEN:PDIF-CN₂ at 70 °C. PL intensities are normalized to the donors' intensities. The insets show zoomed-in subgap regions containing the CT absorption bands. The dotted lines show the Gaussian fit of the lowest CT states. The PL CT bands in (e) and (f) are fitted with one Gaussian for simplicity. The spectra in (e)–(h) are offset for clarity.

strength of the excitations in PDIR-CN₂ along the in-plane direction (as well as in the out-of-plane direction as shown in the Supporting Information, Figure S4) is higher than that in PEN, and therefore a contribution of PDIR-CN₂ dominates the resulting spectra of the blends. In contrast, when mixing with PDIF-CN₂ (Figure 5d), modification of the optical response is observed again. Excitons generated in PEN:PDIF-CN₂ seem to be more broadened compared to those in DIP systems because single transitions are not distinguishable between 2.0 and 2.4 eV (energy range corresponds to the first transitions of PEN and PDIF-CN₂ in solution) in 1:1 and 1:3 mixtures. The spectrum broadening may stem from vibronic coupling which can induce hybrid states between the lowest local-excitation and CT states.⁷⁷ Another reason might be variations of structural conformations leading to multiple transitions with slightly different energies. Emergence of a subgap absorption band, although weaker in comparison with DIP mixtures, is also found. The band starts at around 1.0 eV; i.e., the difference with the DIP systems of ~0.5 eV is consistent with the lower-lying HOMO level of DIP (Figure 1). A detailed interpretation of the energies of the CT states E_{CT} in all four systems is provided in the “Discussion” section.

Photoluminescence Spectroscopy. PL spectra measured at RT are shown in Figure 5e–h. The changes upon cooling down to liquid nitrogen temperature are included in the Supporting Information, Figures S5 and S6. DIP mixtures (Figure 5e,f) reveal strong quenching of the singlet exciton emission and an appearance of a typical CT peak around 1.4

eV. Interestingly, when the molecules are evenly distributed within a film without pure phases, which is the case for equimolar blends in both systems and 3:1 and 1:3 DIP:PDIF-CN₂ films at RT (Supporting Information, Figures S2b and S5b), only the CT emission is maintained. In other cases, when segregation of a pure phase is observed, the emission between 1.6 and 2.2 eV indicates crystallites of the excess component. An emission quenching often is characteristic of face-to-face arrangement and beneficial for solar cell applications because of reduced recombination rates.^{78,79} However, the ultrafast relaxation within the CT band competes with the dissociation process into charge carriers⁸⁰ contributing to the energy loss enhancement unless the lowest CT state is weakly bound.² The latter is rarely the case with face-to-face orientation. In contrast, highly emissive PDIR-CN₂ fully dominates a spectrum when mixed with PEN (Figure 5g). PEN features are distinguishable only in the 3:1 film, since the photoluminescence intensity from PEN is originally a few orders of magnitude weaker. In agreement with the results described above, no evidence for intermolecular coupling can be found in PEN:PDIR-CN₂. Although PDIF-CN₂, similar to PDIR-CN₂, exhibits strong emission, upon intermixing with PEN a decrease of the intensity by 2 orders of magnitude is seen in Figure 5h. We note that in the mixtures a band shape of the residual emission resembles the PDIF-CN₂ monomer spectrum and not that of the thin film. Due to the limits of the instrument, the energy range below 1.2 eV cannot be explored, i.e. the region where, judging from the absorption data, a

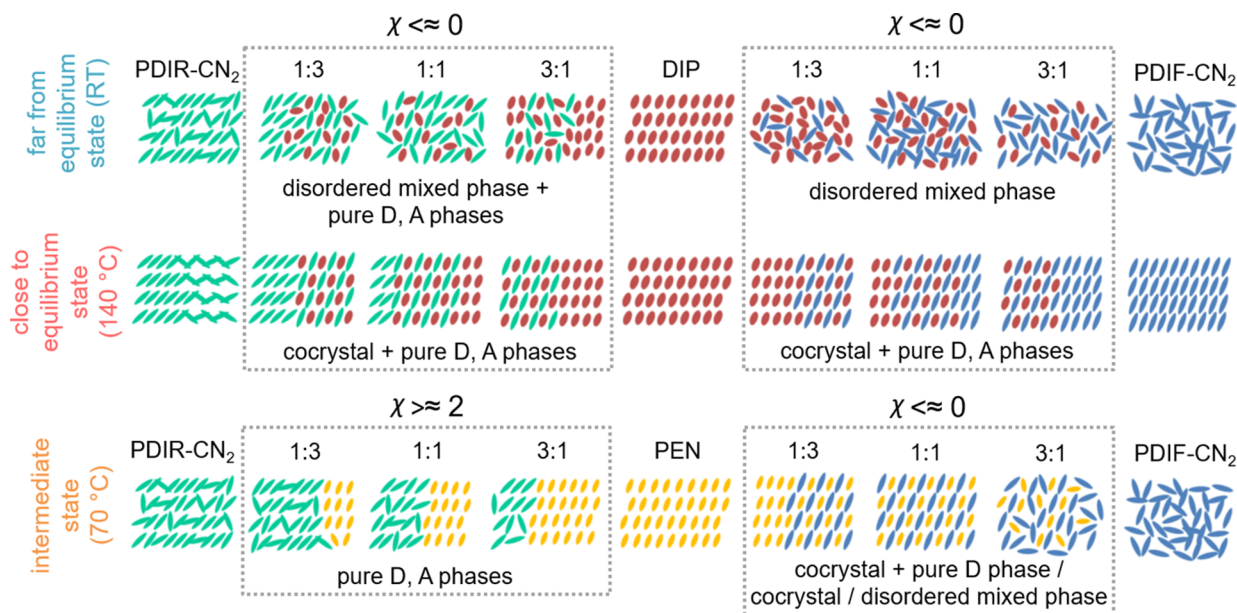


Figure 6. Sketches illustrating mixing behaviors and molecular orientations with respect to the growth direction (vertical in the picture) in DIP (two upper rows) and PEN (bottom row) mixtures in association with the interaction parameter χ .

possible CT emission would be expected. However, the available data along with the FTIR measurements (Figure 4) provide sufficient evidence of CT in PEN:PDIF-CN₂ mixed films.

A precise evaluation of the E_{CT} has been performed in our previous study for DIP:PDIF-CN₂.⁵⁷ Here, we use DIP:PDIF-CN₂ as a reference and estimate the E_{CT} for the rest of the systems from the spectral shift of the lowest CT. The approximate corresponding E_{CT} can be estimated using a simplified approach: $E_{CT} = \frac{1}{2}(E_{CT}^{abs} + E_{CT}^{PL})$. For this, the CT absorption bands were fitted by a sum of Gaussians assuming multiple transitions for each CT band (insets in Figure 5a,b,d; note that only the lowest peak is shown). The PL bands in Figure 5e,f were fitted with a single Gaussian for the sake of simplicity; however, a more complex structure is possible. This results in $E_{CT}^{DIP:PDIF} = 1.50$ eV (consistent with the previous study on RT-deposited films)⁵⁷ and $E_{CT}^{DIP:PDIF} = 1.45$ eV. For PEN:PDIF-CN₂, $E_{CT}^{PEN:PDIF} = 0.95$ eV is estimated from a shift of the CT absorption band with respect to DIP systems.

DISCUSSION

In this paper, we compare interactions and formation of CT complexes for combinations of donor–acceptor molecules with different sterical properties and electronic structure. We split the discussion into two key issues: (1) the correlation between structure and CT state observation and (2) the chain modification for tuning the ground state energy levels.

Essentially, two main parameters are examined: the structural compatibility due to the molecular geometry and the energy gap E_{DA} . In three D/A systems the observation of a CT complex correlates with intermixing of the molecular components accompanied by a mixed phase formation during film deposition, whereas the strongly segregating system preserves the structural and optical characteristics of both moieties. However, the mixing vs. demixing scenario is apparently determined by the molecular tendency to intermolecular coupling. The intermolecular interactions

between D and A are not necessarily based on CT in the ground electronic state, although it is apparently present to some extent in the systems studied, as evidenced by FTIR (Figure 4).

Here, we suggest considering the mixing scenarios between the small molecule materials studied in terms of a nearest-neighbor interaction model, where the main driving force of nucleation is the difference between host–host (W_{AA}), guest–guest (W_{BB}), and host–guest (W_{AB}) intermolecular interactions:⁸¹

$$\chi = \frac{Z}{k_B T} (W_{AA} + W_{BB} - 2W_{AB}) \quad (1)$$

where χ is the interaction parameter, Z is the coordination number, k_B is the Boltzmann constant, and T is the temperature.

The balance of χ coupled with the entropy contribution governs the possible mixing scenarios: in the case of all energies W being similar ($\chi \approx 0$), there is no preferred interaction in the system, which leads to formation of a solid solution or statistical mixing; when any of the W terms dominates, the corresponding phase tends to separate whether it is a pure phase A or B ($\chi > 2$) or an AB cocrystal ($\chi < 0$).

Equation 1 defines the equilibrium state of the system. We emphasize that this is a simplified model aimed at rationalizing the data but not the full picture. Inter alia, anisotropies and nonequilibrium effects are not considered, despite their obvious importance.⁸² The thin film deposition process introduces kinetic effects that often “freeze” the system in a disordered nonequilibrium state. A higher T_{sub} increases the molecular diffusion length, which brings the system closer to the equilibrium state. We note that the entropy increase, which would favor intermixing, due to an increase of temperature, is not relevant in our parameter range.

On the basis of the above data, the proposed microstructures are visually summarized in Figure 6. The top row shows the mixing behavior in DIP systems at RT. For PDIF-CN₂, the films are nearly amorphous for T_{sub} below ~ 110 – 120 °C. The

PDIF-CN₂ films are weakly crystalline due to the shielding effect of the side chains, as opposed to DIP and PEN. Thus, $W_{\text{PDIF-PDIF}}$ is most likely smaller than $W_{\text{PDIF-PDIR}}$, $W_{\text{DIP-DIP}}$, and $W_{\text{PEN-PEN}}$. This allows PDIF-CN₂ molecules to easily intermix with sterically compatible DIP molecules. The disruptive influence of PDIF-CN₂ molecules leads to a decrease in the long-range order in blends with an excess of DIP at RT (Supporting Information, Figure S2b). This leads to the formation of a solid solution (and an absence of the preferred crystal packing) with the properties of the CT complex even for nonequimolar films (Supporting Information, Figure S5b). Nucleation of the PDIF-CN₂ crystalline phase occurs at HT when the higher kinetic energies enable the formation of a stabilizing π - π interaction between the perylene diimide backbones. In the mixed film the higher temperature results in the coexistence of the pristine and mixed crystal phases. The strength of the CT-complex-related optical features such as the absorption and emission bands correlates directly with the cocrystal grain size which increases with T_{sub} (Supporting Information, Figures S7–S10).

Among the material combinations studied, the intermolecular interactions between DIP and PDIR-CN₂ seem to be the strongest. We find pronounced crystallinity at RT, since the alkyl side chains have a weaker hindering effect on PDIR-CN₂ intermolecular coupling in comparison to the fluorinated chains. Consequently, phase separation in DIP:PDIR-CN₂ is observed at RT in contrast to DIP:PDIF-CN₂. HT assists in formation of the highly crystalline extended 1D D/A packing. Typically, for small aromatic molecules, in particular for rod-like molecules, a face-centered parallel stacking is disfavored, in contrast to T-shaped or offset-stacked geometries (herringbone structure as a compromise) due to electrostatic repulsion.^{83,84} This is the case unless electrostatic interaction of donor (electron-donating) and acceptor (electron-withdrawing) species contributes to the balance of the interactions, making a face-centered stacking the most-observed D/A cocrystal geometry.^{68,69,79}

While the mixing scenario can be rationalized using eq 1, the phase evolution is a result of a complex interplay of kinetic parameters such as diffusion, mobility, deposition rate, and temperature.^{85–87} It has been observed that elevated processing temperatures facilitate demixing of chemically or sterically incompatible molecules.⁸⁸ At HT even a slight deviation from the 1:1 stoichiometry induces nucleation of the pure phase of the respective excess species. The results provide an option to maintain both mixed and pristine phases when the increased crystallinity is achieved, while at RT all mixed phases studied are weakly ordered and resemble a statistic mixture, which seems to strongly limit the charge carrier mobility.^{32,57,89}

PEN is apparently sterically less compatible with the larger PDI, and the area of the aromatic system constituting the backbone is too small.⁴⁰ As a consequence, the phase-separating PEN:PDIR-CN₂ is the only system where neither GS-CT nor ES-CT is observed. Intermixing of PEN with PDIF-CN₂ is possible owing to the weak $W_{\text{PDIF-PDIF}}$ coupling which is partly suppressed by the shielding effect of the fluorinated side chains. However, the pure PEN phase persists in 3:1 and likely even in 1:1 mixtures. With the further increase of PDIF-CN₂ content the mixed phase experiences dilution within the amorphous matrix.

The free energies of the mixed films vs mixing ratio are sketched in a simplified schematic energy diagram in Figure 7. The donor–acceptor component is favored for highly

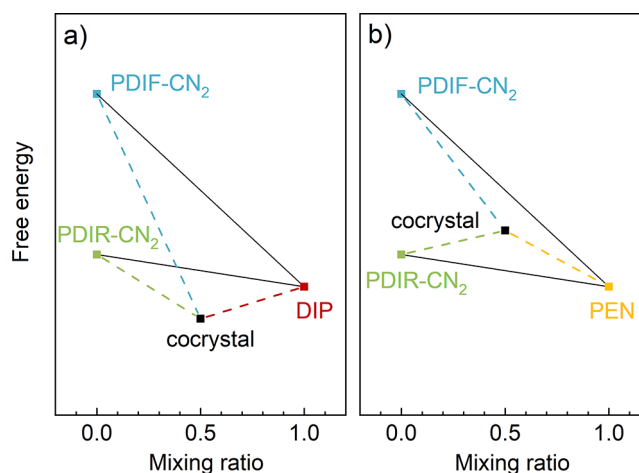


Figure 7. Simplified sketch of the energetically beneficial cocrystal formation in the cases of DIP:PDIR-CN₂ and DIP:PDIF-CN₂ (a) and PEN:PDIF-CN₂ (b). Solid black lines correspond to the free energy for complete phase separation of the two compounds. Dashed lines correspond to the free energy of a 1:1 cocrystal with phase separated pure compound. For mixtures with DIP (a), we find that the formation of the cocrystal is energetically favored for both systems. For mixtures with PEN, we find that the cocrystal formation is energetically less stable due to steric hindrances; therefore we find cocrystal formation only for the PEN:PDIF-CN₂ system. Note that we assume that the energies for mixing (cocrystal) for each donor with the two PDI derivatives are similar because the intermolecular interaction is located mostly on the identical PDI core.

compatible DIP:PDIs and less compatible PEN:PDIF-CN₂. Therefore, for these three systems, the cocrystal in the diagram refers to an energetically more stable structure in comparison with the complete phase separation. $W_{\text{PEN:PDIF}}$ is sufficient to overcompensate the weak $W_{\text{PDIF:PDIF}}$, and therefore a free energy gain is achieved by formation of the cocrystal. An increase in the binding energy in mixed binary films was also measured earlier for a different but related system (PEN:PFP) by thermal desorption spectroscopy.⁹⁰ However, the PDIR-CN₂ phase is energetically more stable than the PDIF-CN₂ phase and does not follow this scenario (Figure 7b).

As a second key question, we discuss whether a tuning of the energy levels by different side chains also allows the tuning of the CT energy. In this work, by “CT energy” we refer to an energy of the lowest (“relaxed”) levels in a CT state manifold, which can participate in the CT exciton generation and recombination via a direct electronic transition.^{1–3,91} The energy levels measured in the pristine films are summarized in Figure 8 (left). Note that all values refer to films grown at RT.^{48,55–57} The largest E_{DA} seems to be between DIP and PDIR-CN₂, followed by DIP and PDIF-CN₂, and the smallest one is supposed to be between PEN and PDIF-CN₂. However, as discussed in ref 48, the energy shift between PDIR-CN₂ and PDIF-CN₂ thin films originates from the polarization effect of the fluorinated side chains exhibiting higher electron density in comparison with the perylene diimide backbone, whereas the electronic structure of the monomers in the absence of this environmental effects stays similar. The sketch in the Supporting Information, Figure S11 illustrates how the photoelectron kinetic energy measured by UPS is affected by the surface dipole moment created by the difference in the electron density of the fluorinated side chains and the aromatic core.^{92–94}

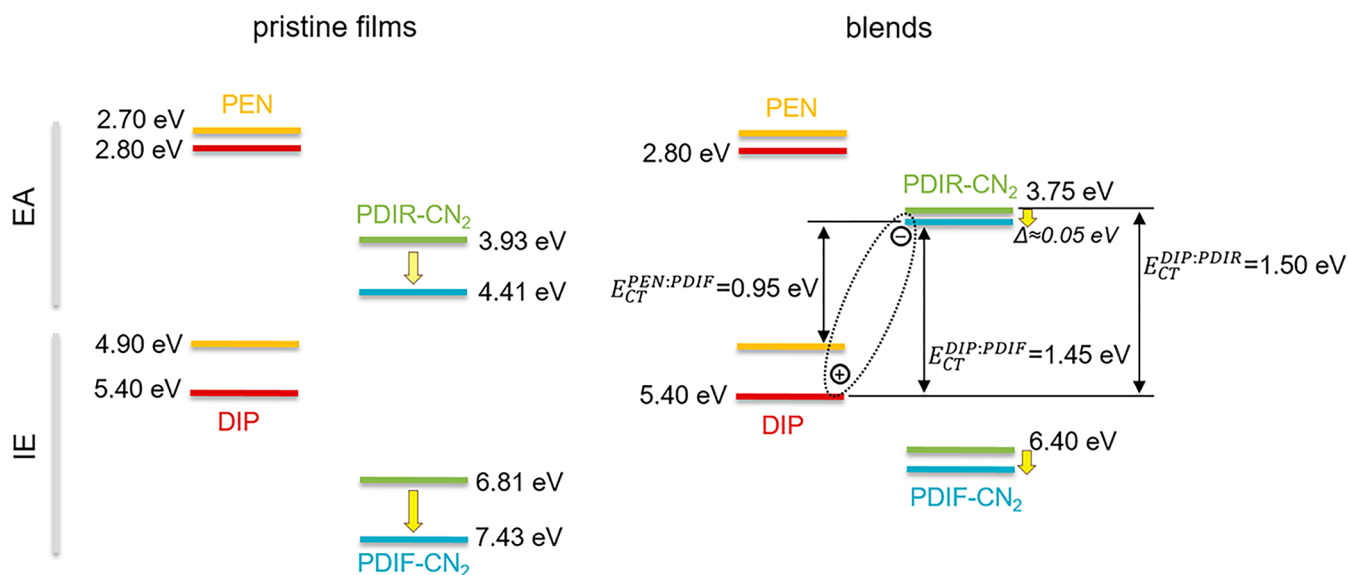


Figure 8. Energy level diagrams for the pristine films (left) and the D/A blends (right). The yellow arrows are guides for the eye for the energy shift between PDIR-CN₂ and PDIF-CN₂. The CT energies (except for DIP:PDIR-CN₂) are based on the optical data.

This can be an explanation why, despite the fact that the different side substituents affect the thin film structural and optical properties (Figure 5a,b), the resulting D/A complexes exhibit almost identical energy landscapes in DIP:PDIR-CN₂ and DIP:PDIF-CN₂. The energy levels in the DIP:PDIR-CN₂ mixture defined in ref 57 are taken here as a reference for the other systems where the corresponding shifts are estimated using the CT-energies from Figure 5. Thus, the CT state energies differ by about 0.05 eV for DIP:PDIF-CN₂ as shown in Figure 8 (right), which is significantly smaller than the measured difference in the EA for the pristine acceptor thin films. Furthermore, the oscillator strength of the CT optical features seems to correlate with the quality of the cocrystal (Supporting Information, Figures S7–S10), which is best in the case of DIP:PDIR-CN₂ grown at 140 °C. Thus, the main idea is that the CT complex seems to be localized mostly on DIP and on the PDI backbone, and since the CT transition is anisotropic and oriented parallel to the π - π stacking, the perfluorination of side chains therefore shifts the energy levels of the thin film, though the face-to-face interaction of both compounds seems to be mostly unaffected by the substitution.

The replacement of DIP by PEN, a molecule with a different backbone structure, causes alterations in the intermolecular coupling, which is present in PEN:PDIF-CN₂, including formation of a CT complex, but it is absent in phase-separating PEN:PDIR-CN₂. The CT features in PEN:PDIF-CN₂ are less prominent compared to the DIP systems. The higher PEN HOMO level results in the corresponding red-shift of the CT states ($E_{CT} \approx 0.95$ eV in Figure 8, right). However, this does not ensure formation of a “stronger” CT complex with predominantly hybridized molecular orbitals as evidenced by both UV/vis and FTIR data, at least as long as the structure influence is excluded.

Along with the steric compatibility and the energy variability, we find another aspect worth mentioning, namely, the relative orientation of the dipole moment of the first HOMO–LUMO transition μ (depicted by yellow arrows in Figure 1) which shows the direction of the highest excitation probability. Here, we briefly discuss whether the relative orientation of the intramolecular μ may influence the

intermolecular CT transition. The orientation of μ corresponds to the asymmetry of the product of the frontier orbital wave functions.^{95,96} As was shown recently, a CT transition can be anisotropic and tends to occur in a direction perpendicular to the orientation of the donor and acceptor π -conjugated core plane (at least for relatively flat and rod-like compounds with the ordering motif as found for the compounds under investigation here).^{57,97} Thus, under excitation an electron of a donor might be transferred by one of the two competing electronic transitions: either within the molecular plane into one of the excited states, or perpendicular to that into the CT state. In the cocrystals studied, D/A molecules have their long axis predominantly aligned parallel to the substrate normal, therefore the considerable oscillator strength of the CT transitions is observed in the in-plane direction (parallel to the substrate) in Figure 5. Among the chosen compounds, DIP and PDIR-CN₂ represent a D/A couple with parallel transition dipole moments oriented along the long molecular axis. In a PEN molecule μ is oriented along the short molecular axis,⁹⁸ which one might consider as one of the possible reasons for the lower oscillator strength of the CT transition in PEN:PDIF-CN₂ system (Figure 5).

A number of theoretical models were developed in the past in order to describe a possible interference between Frenkel and CT states.^{99–102} These excitations are considered to be coupled via electron and hole transfer in case of ordered molecular stacks. On the basis of these models, one could consider that there might be small admixtures of HOMO_A in HOMO_D, and CT transition dipole moments based on HOMO_D and LUMO_A would contain the respective amounts of intramolecular transition dipoles. However, quantitatively, the effect of borrowing of oscillator strength is difficult to observe since the area below the CT transitions in Figure 5a,b,d is of the order of 1% of the total area of $\epsilon_{2,xy}$. Thereby, a possible contamination between the frontier orbitals of donor and acceptor seems to have little impact on a changed visibility of the CT transition, allowing us to claim that this contamination remains small and that we observe a nearly pure CT state. In addition, judging from the out-of-plane absorption data obtained from ellipsometry (Supporting

Information, Figure S4), we do not find any oscillator strength of the CT transitions in the out-of-plane direction for all studied mixed systems. From this observation, we conclude that the orientation of the CT transition is in all our cases in-plane and independent of the orientation of μ in the pure compounds.

CONCLUSION

To conclude, the results show a direct correlation between small molecule compatibility for mixing and the CT properties of the corresponding D/A complex. The sterical, structural, and energetic factors are analyzed and summarized in a simplified scheme. The morphology of a small molecule D/A mixture can be controlled by tailoring the intermolecular interactions via change of molecular geometry and/or T_{sub} . PDI acceptors reveal better structural compatibility with perylene-based DIP than with PEN. In our schematic representation, intermolecular interactions are an essential parameter determining the possible mixing scenarios. The electrostatic component between D and A molecules plays an important role in the energy balance. Therefore, the 1D D/A face-centered stacking is preferred which is hardly achievable between like molecules.

At the same time, the formation of a CT complex is a function of the film structure and the energy gap E_{DA} , but apparently is not essentially influenced by the intramolecular excitations. In the phase-separating system (PEN:PDIF-CN₂) no evidence of intermolecular coupling between D and A species are observed. This contrasts with all three intermixing systems, for which clear indications of the CT in both ground and excited electronic states were found. The typical indications are a similar shift of the characteristic vibration mode in the FTIR spectra, appearance of the CT subgap absorption band along with the hybrid spectrum of the first “main” optical absorption band, and the strong luminescence quenching. The oscillator strength of the optical CT features (both for absorption and emission) strongly correlates with the quality of the cocrystal, which can be controlled by the deposition temperature and the strength of the intermolecular attractive interaction. We have shown that fluorination of the side chains in the PDIs leads to a shift of the measured IE and EA due to molecule polarization, however, their frontier orbitals are not necessarily strongly affected. Since the CT transition is anisotropic, its energy does not change significantly when replacing the acceptor. The aromatic core stays the same and the side chains do not take part in the CT complex formation. However, replacement of the DIP donor with PEN leads to the corresponding change in the CT energy. The results underline the importance of correlations between structural/sterical issues and CT and contribute to development of the cocrystal engineering.⁴⁵

ASSOCIATED CONTENT

Supporting Information

The Supporting Information is available free of charge at <https://pubs.acs.org/doi/10.1021/acs.jpcc.0c00230>.

X-ray diffraction of different mixing ratios of DIP:PDIF-CN₂, DIP:PDIF-CN₂, and PEN:PDIF-CN₂ series grown at elevated T_{sub} as well as DIP blends grown at room temperature; ellipsometry out-of-plane results; photoluminescence data measured at 77 K; DRS on 1:1

mixtures; structure–CT properties in DIP:PDIF-CN₂; sketch of the polarization effect on UPS data (PDF)

AUTHOR INFORMATION

Corresponding Authors

Valentina Belova – *Institut für Angewandte Physik, Universität Tübingen, 72076 Tübingen, Germany*; orcid.org/0000-0002-8142-2090; Email: vbelova@icmab.es

Alexander Hinderhofer – *Institut für Angewandte Physik, Universität Tübingen, 72076 Tübingen, Germany*; orcid.org/0000-0001-8152-6386; Email: alexander.hinderhofer@uni-tuebingen.de

Authors

Clemens Zeiser – *Institut für Angewandte Physik, Universität Tübingen, 72076 Tübingen, Germany*

Timo Storzer – *Institut für Angewandte Physik, Universität Tübingen, 72076 Tübingen, Germany*

Jakub Rozbořil – *CEITEC, Masaryk University and Department of Condensed Matter Physics, Faculty of Science, Masaryk University, CZ-611 37 Brno, Czech Republic*

Jan Hagenlocher – *Institut für Angewandte Physik, Universität Tübingen, 72076 Tübingen, Germany*

Jiří Novák – *CEITEC, Masaryk University and Department of Condensed Matter Physics, Faculty of Science, Masaryk University, CZ-611 37 Brno, Czech Republic*; orcid.org/0000-0003-4664-746X

Alexander Gerlach – *Institut für Angewandte Physik, Universität Tübingen, 72076 Tübingen, Germany*; orcid.org/0000-0003-1787-1868

Reinhard Scholz – *Leibniz-Institut für Polymerforschung Dresden e. V., 01069 Dresden, Germany*; orcid.org/0000-0003-3528-5475

Frank Schreiber – *Institut für Angewandte Physik, Universität Tübingen, 72076 Tübingen, Germany*; orcid.org/0000-0003-3659-6718

Complete contact information is available at: <https://pubs.acs.org/doi/10.1021/acs.jpcc.0c00230>

Author Contributions

The manuscript was written through contributions of all authors. All authors have given approval to the final version of the manuscript.

Notes

The authors declare no competing financial interest.

ACKNOWLEDGMENTS

We acknowledge that this research was financially supported by the Deutsche Forschungsgemeinschaft (Grants SCHR 700/20-1 and HI 1927/1-1). J.N. and J.R. acknowledge support from Project CEITEC 2020 (Grant LQ1601 financed by the MEYS of the Czech Republic) and DAAD/AWTR/MEYS (Grant 57215815/7AMB16DE006). We are grateful for the beam times granted by the ESRF (Grenoble, France) and Soleil (Paris, France) and helpful assistance of the staff of the ID10 (Andrey Chumakov and Oleg Kononov, ESRF) and SixS (Alina Vlad, Soleil) beamlines. We thank Katharina Broch, Rupak Banerjee, and Lisa Egenberger for help during synchrotron beam times.

REFERENCES

- (1) Vandewal, K. Interfacial Charge Transfer States in Condensed Phase Systems. *Annu. Rev. Phys. Chem.* **2016**, *67*, 113–133.
- (2) Vandewal, K.; Albrecht, S.; Hoke, E. T.; Graham, K. R.; Widmer, J.; Douglas, J. D.; Schubert, M.; Mateker, W. R.; Bloking, J. T.; Burkhard, G. F.; et al. Efficient Charge Generation by Relaxed Charge-Transfer States at Organic Interfaces. *Nat. Mater.* **2014**, *13*, 63–68.
- (3) Deibel, C.; Strobel, T.; Dyakonov, V. Role of the Charge Transfer State in Organic Donor–Acceptor Solar Cells. *Adv. Mater.* **2010**, *22*, 4097–4111.
- (4) Coropceanu, V.; Chen, X. K.; Wang, T.; Zheng, Z.; Brédas, J. L. Charge-Transfer Electronic States in Organic Solar Cells. *Nat. Rev. Mater.* **2019**, *4*, 689–707.
- (5) Paraschuk, D. Y.; Elizarov, S. G.; Khodarev, A. N.; Shchegolikhin, A. N.; Arnavtsov, S. A.; Nechvolodova, E. M. Weak Intermolecular Charge Transfer in the Ground State of a π -Conjugated Polymer Chain. *JETP Lett.* **2005**, *81*, 467–470.
- (6) Hwang, I. W.; Cho, S.; Kim, J. Y.; Lee, K.; Coates, N. E.; Moses, D.; Heeger, A. J. Carrier Generation and Transport in Bulk Heterojunction Films Processed with 1,8-Octanedithiol as a Processing Additive. *J. Appl. Phys.* **2008**, *104*, 033706.
- (7) Brabec, B. C. J.; Cravino, A.; Meissner, D.; Sariciftci, N. S.; Fromherz, T.; Rispsen, M. T.; Sanchez, L.; Hummel, J. C. Origin of the Open Circuit Voltage of Plastic Solar Cells. *Adv. Funct. Mater.* **2001**, *11*, 374–380.
- (8) Cremer, J.; Bäuerle, P.; Wienk, M. M.; Janssen, R. A. J. High Open-Circuit Voltage Poly (Ethylnylene Bithienylene):Fullerene Solar Cells. *Chem. Mater.* **2006**, *18*, 5832–5834.
- (9) Kim, H.; Kim, J. Y.; Park, S. H.; Lee, K.; Jin, Y.; Kim, J.; Suh, H. Electroluminescence in Polymer-Fullerene Photovoltaic Cells. *Appl. Phys. Lett.* **2005**, *86*, 183502.
- (10) Brütting, W.; Adachi, C. *Physics of Organic Semiconductors*, 2nd ed.; Wiley-VCH: Weinheim, Germany, 2012.
- (11) Zieleniewska, A.; Lodermeier, F.; Roth, A.; Guldi, D. M. Fullerenes-How 25 Years of Charge Transfer Chemistry Have Shaped Our Understanding of (Interfacial) Interactions. *Chem. Soc. Rev.* **2018**, *47*, 702–714.
- (12) Eftaiha, A. F.; Sun, J.-P.; Hill, I. G.; Welch, G. C. Recent Advances of Non-Fullerene, Small Molecular Acceptors for Solution Processed Bulk Heterojunction Solar Cells. *J. Mater. Chem. A* **2014**, *2*, 1201–1213.
- (13) Anthony, J. E. Small-Molecule, Nonfullerene Acceptors for Polymer Bulk Heterojunction Organic Photovoltaics. *Chem. Mater.* **2011**, *23*, 583–590.
- (14) Wu, C. H.; Chueh, C. C.; Xi, Y. Y.; Zhong, H. L.; Gao, G. P.; Wang, Z. H.; Pozzo, L. D.; Wen, T. C.; Jen, A. K. Y. Influence of Molecular Geometry of Perylene Diimide Dimers and Polymers on Bulk Heterojunction Morphology Toward High-Performance Non-fullerene Polymer Solar Cells. *Adv. Funct. Mater.* **2015**, *25*, 5326–5332.
- (15) Scharber, M. C. On the Efficiency Limit of Conjugated Polymer:Fullerene-Based Bulk Heterojunction Solar Cells. *Adv. Mater.* **2016**, *28*, 1994–2001.
- (16) Shi, J.; Isakova, A.; Abudulimu, A.; van den Berg, M.; Kwon, O. K.; Meixner, A. J.; Park, S. Y.; Zhang, D.; Gierschner, J.; Luer, L. Designing High Performance All-Small Molecule Solar Cells with Non-Fullerene Acceptors: Comprehensive Studies on Photoexcitation Dynamics and Charge Separation Kinetics. *Energy Environ. Sci.* **2018**, *11*, 211–220.
- (17) Lin, Y.; Wang, J.; Zhang, Z. G.; Bai, H.; Li, Y.; Zhu, D.; Zhan, X. An Electron Acceptor Challenging Fullerenes for Efficient Polymer Solar Cells. *Adv. Mater.* **2015**, *27*, 1170–1174.
- (18) Tang, A.; Xiao, B.; Wang, Y.; Gao, F.; Tajima, K.; Bin, H.; Zhang, Z. G.; Li, Y.; Wei, Z.; Zhou, E. Simultaneously Achieved High Open-Circuit Voltage and Efficient Charge Generation by Fine-Tuning Charge-Transfer Driving Force in Nonfullerene Polymer Solar Cells. *Adv. Funct. Mater.* **2018**, *28*, 1704507.
- (19) Yuan, J.; Zhang, Y.; Zhou, L.; Zhang, G.; Yip, H. L.; Lau, T. K.; Lu, X.; Zhu, C.; Peng, H.; Johnson, P. A.; et al. Single-Junction Organic Solar Cell with over 15% Efficiency Using Fused-Ring Acceptor with Electron-Deficient Core. *Joule* **2019**, *3*, 1140–1151.
- (20) Miao, J.; Meng, B.; Liu, J.; Wang, L. An A-D-A'-D-A Type Small Molecule Acceptor with a Broad Absorption Spectrum for Organic Solar Cells. *Chem. Commun.* **2018**, *54*, 303–306.
- (21) Isaacs, E. B.; Sharifzadeh, S.; Ma, B.; Neaton, J. B. Relating Trends in First-Principles Electronic Structure and Open-Circuit Voltage in Organic Photovoltaics. *J. Phys. Chem. Lett.* **2011**, *2*, 2531–2537.
- (22) Benduhn, J.; Tvingstedt, K.; Piersimoni, F.; Ullbrich, S.; Fan, Y.; Tropiano, M.; McGarry, K. A.; Zeika, O.; Riede, M. K.; Douglas, C. J.; et al. Intrinsic Non-Radiative Voltage Losses in Fullerene-Based Organic Solar Cells. *Nat. Energy* **2017**, *2*, 17053.
- (23) Hallermann, M.; Da Como, E.; Feldmann, J.; Izquierdo, M.; Filippone, S.; Martin, N.; Jüchter, S.; von Hauff, E. Correlation between Charge Transfer Exciton Recombination and Photocurrent in Polymer/Fullerene Solar Cells. *Appl. Phys. Lett.* **2010**, *97*, 023301.
- (24) Chen, X.-K.; Ravva, M. K.; Li, H.; Ryno, S. M.; Brédas, J.-L. Effect of Molecular Packing and Charge Delocalization on the Nonradiative Recombination of Charge-Transfer States in Organic Solar Cells. *Adv. Energy Mater.* **2016**, *6*, 1601325.
- (25) Clark, J.; Archer, R.; Redding, T.; Foden, C.; Tant, J.; Geerts, Y.; Friend, R. H.; Silva, C. Charge Recombination in Distributed Heterostructures of Semiconductor Discotic and Polymeric Materials. *J. Appl. Phys.* **2008**, *103*, 124510.
- (26) Kendrick, M. J.; Neunzert, A.; Payne, M. M.; Purushothaman, B.; Rose, B. D.; Anthony, J. E.; Haley, M. M.; Ostroverkhova, O. Formation of the Donor-Acceptor Charge-Transfer Exciton and Its Contribution to Charge Photogeneration and Recombination in Small-Molecule Bulk Heterojunctions. *J. Phys. Chem. C* **2012**, *116*, 18108–18116.
- (27) Sarma, M.; Wong, K. T. Exciplex: An Intermolecular Charge-Transfer Approach for TADF. *ACS Appl. Mater. Interfaces* **2018**, *10*, 19279–19304.
- (28) Brown, A. M.; McCusker, C. E.; Carey, M. C.; Blanco-Rodríguez, A. M.; Towrie, M.; Clark, I. P.; Vlček, A.; McCusker, J. K. Vibrational Relaxation and Redistribution Dynamics in Ruthenium-(II) Polypyridyl-Based Charge-Transfer Excited States: A Combined Ultrafast Electronic and Infrared Absorption Study. *J. Phys. Chem. A* **2018**, *122*, 7941–7953.
- (29) Jones, M. L.; Jankowski, E. Computationally Connecting Organic Photovoltaic Performance to Atomistic Arrangements and Bulk Morphology. *Mol. Simul.* **2017**, *43*, 756–773.
- (30) Huang, Y.; Kramer, E. J.; Heeger, A. J.; Bazan, G. C. Bulk Heterojunction Solar Cells: Morphology and Performance Relationships. *Chem. Rev.* **2014**, *114*, 7006–7043.
- (31) Lin, Y. H. L.; Fusella, M. A.; Rand, B. P. The Impact of Local Morphology on Organic Donor/Acceptor Charge Transfer States. *Adv. Energy Mater.* **2018**, *8*, 1702816.
- (32) Fischer, J.; Widmer, J.; Kleemann, H.; Tress, W.; Koerner, C.; Riede, M.; Vandewal, K.; Leo, K. A Charge Carrier Transport Model for Donor-Acceptor Blend Layers. *J. Appl. Phys.* **2015**, *117*, 045501.
- (33) Shoaee, S.; Subramanian, S.; Xin, H.; Keiderling, C.; Tuladhar, P. S.; Jamieson, F.; Jenekhe, S. A.; Durrant, J. R. Charge Photogeneration for a Series of Thiazolo-Thiazole Donor Polymers Blended with the Fullerene Electron Acceptors PCBM and ICBA. *Adv. Funct. Mater.* **2013**, *23*, 3286–3298.
- (34) Zusan, A.; Vandewal, K.; Allendorf, B.; Hansen, N. H.; Pflaum, J.; Salleo, A.; Dyakonov, V.; Deibel, C. The Crucial Influence of Fullerene Phases on Photogeneration in Organic Bulk Heterojunction Solar Cells. *Adv. Energy Mater.* **2014**, *4*, 1400922.
- (35) Kraner, S.; Scholz, R.; Koerner, C.; Leo, K. Design Proposals for Organic Materials Exhibiting a Low Exciton Binding Energy. *J. Phys. Chem. C* **2015**, *119*, 22820–22825.
- (36) Opitz, A.; Wagner, J.; Brütting, W.; Hinderhofer, A.; Schreiber, F. Molecular Semiconductor Blends: Microstructure, Charge Carrier

Transport, and Application in Photovoltaic Cells. *Phys. Status Solidi A* **2009**, *206*, 2683–2694.

(37) Zhang, Y.; Sajjad, M. T.; Blaszczyk, O.; Parnell, A. J.; Ruseckas, A.; Serrano, L. A.; Cooke, G.; Samuel, I. D. W. Large Crystalline Domains and an Enhanced Exciton Diffusion Length Enable Efficient Organic Solar Cells. *Chem. Mater.* **2019**, *31*, 6548–6557.

(38) Lunt, R. R.; Benziger, J. B.; Forrest, S. R. Relationship between Crystalline Order and Exciton Diffusion Length in Molecular Organic Semiconductors. *Adv. Mater.* **2010**, *22*, 1233–1236.

(39) Hinderhofer, A.; Schreiber, F. Organic–Organic Heterostructures: Concepts and Applications. *ChemPhysChem* **2012**, *13*, 628–643.

(40) Vogel, J.-O.; Salzmann, I.; Duhm, S.; Oehzelt, M.; Rabe, J. P.; Koch, N. Phase-Separation and Mixing in Thin Films of Co-Deposited Rod-like Conjugated Molecules. *J. Mater. Chem.* **2010**, *20*, 4055–4066.

(41) Dieterle, J.; Broch, K.; Frank, H.; Duva, G.; Storzer, T.; Hinderhofer, A.; Novák, J.; Gerlach, A.; Schreiber, F. Delayed Phase Separation in Growth of Organic Semiconductor Blends with Limited Intermixing. *Phys. Status Solidi RRL* **2017**, *11*, 1600428.

(42) Fenter, P.; Schreiber, F.; Zhou, L.; Eisenberger, P.; Forrest, S. R. In Situ Studies of Morphology, Strain, and Growth Modes of a Molecular Organic Thin Film. *Phys. Rev. B: Condens. Matter Mater. Phys.* **1997**, *56*, 3046–3053.

(43) Dieterle, J.; Broch, K.; Hinderhofer, A.; Frank, H.; Novák, J.; Gerlach, A.; Breuer, T.; Banerjee, R.; Witte, G.; Schreiber, F. Structural Properties of Picene-Perfluoropentacene and Picene-Pentacene Blends: Superlattice Formation versus Limited Intermixing. *J. Phys. Chem. C* **2015**, *119*, 26339–26347.

(44) Reinhardt, J. P.; Hinderhofer, A.; Broch, K.; Heinemeyer, U.; Kowarik, S.; Vorobiev, A.; Gerlach, A.; Schreiber, F. Structural and Optical Properties of Mixed Diindenoperylene–Perfluoropentacene Thin Films. *J. Phys. Chem. C* **2012**, *116*, 10917–10923.

(45) Sun, L.; Zhu, W.; Yang, F.; Li, B.; Ren, X.; Zhang, X.; Hu, W. Molecular Cocrystals: Design, Charge-Transfer and Optoelectronic Functionality. *Phys. Chem. Chem. Phys.* **2018**, *20*, 6009–6023.

(46) Ferlauto, L.; Liscio, F.; Orgiu, E.; Masciocchi, N.; Guagliardi, A.; Biscarini, F.; Samori, P.; Milota, S. Enhancing the Charge Transport in Solution-Processed Perylene Di-Imide Transistors via Thermal Annealing of Metastable Disordered Films. *Adv. Funct. Mater.* **2014**, *24*, 5503–5510.

(47) Jones, B. A.; Ahrens, M. J.; Yoon, M. H.; Facchetti, A.; Marks, T. J.; Wasielewski, M. R. High-Mobility Air-Stable n-Type Semiconductors with Processing Versatility: Dicyanoperylene-3,4,9,10-Bis(Dicarboximides). *Angew. Chem.* **2004**, *116*, 6523–6526.

(48) Belova, V.; Wagner, B.; Reisz, B.; Zeiser, C.; Duva, G.; Rozbõřil, J.; Novák, J.; Gerlach, A.; Hinderhofer, A.; Schreiber, F. Real-Time Structural and Optical Study of Growth and Packing Behavior of Perylene Diimide Derivative Thin Films: The Influence of Side-Chain Modification. *J. Phys. Chem. C* **2018**, *122*, 8589–8601.

(49) Wong, S. L.; Huang, H.; Huang, Y. L.; Wang, Y. Z.; Gao, X. Y.; Suzuki, T.; Chen, W.; Wee, A. T. S. Effect of Fluorination on the Molecular Packing of Perfluoropentacene and Pentacene Ultrathin Films on Ag (111). *J. Phys. Chem. C* **2010**, *114*, 9356–9361.

(50) Wagner, J.; Gruber, M.; Hinderhofer, A.; Wilke, A.; Bröker, B.; Frisch, J.; Amsalem, P.; Vollmer, A.; Opitz, A.; Koch, N.; et al. High Fill Factor and Open Circuit Voltage in Organic Photovoltaic Cells with Diindenoperylene as Donor Material. *Adv. Funct. Mater.* **2010**, *20*, 4295–4303.

(51) Gruber, M.; Rawolle, M.; Wagner, J.; Magerl, D.; Hörmann, U.; Perlich, J.; Roth, S. V.; Opitz, A.; Schreiber, F.; Müller-Buschbaum, P.; et al. Correlating Structure and Morphology to Device Performance of Molecular Organic Donor–Acceptor Photovoltaic Cells Based on Diindenoperylene (DIP) and C60. *Adv. Energy Mater.* **2013**, *3*, 1075–1083.

(52) Yoo, S.; Domercq, B.; Kippelen, B. Efficient Thin-Film Organic Solar Cells Based on Pentacene/C60 Heterojunctions. *Appl. Phys. Lett.* **2004**, *85*, 5427–5429.

(53) Dimitrakopoulos, C. D.; Brown, A. R.; Pomp, A. Molecular Beam Deposited Thin Films of Pentacene for Organic Field Effect Transistor Applications. *J. Appl. Phys.* **1996**, *80*, 2501–2508.

(54) Feili, D.; Schuettler, M.; Doerge, T.; Kammer, S.; Stieglitz, T. Encapsulation of Organic Field Effect Transistors for Flexible Biomedical Microimplants. *Sens. Actuators, A* **2005**, *120*, 101–109.

(55) Krause, S.; Schöll, A.; Umbach, E. Interplay of Geometric and Electronic Structure in Thin Films of Diindenoperylene on Ag(1 1 1). *Org. Electron.* **2013**, *14*, 584–590.

(56) Han, W.; Yoshida, H.; Ueno, N.; Kera, S. Electron Affinity of Pentacene Thin Film Studied by Radiation-Damage Free Inverse Photoemission Spectroscopy. *Appl. Phys. Lett.* **2013**, *103*, 123303.

(57) Belova, V.; Beyer, P.; Meister, E.; Linderl, T.; Halbich, M. U.; Gerhard, M.; Schmidt, S.; Zechel, T.; Meisel, T.; Generalov, A. V.; et al. Evidence for Anisotropic Electronic Coupling of Charge Transfer States in Weakly Interacting Organic Semiconductor Mixtures. *J. Am. Chem. Soc.* **2017**, *139*, 8474–8486.

(58) Heinemeyer, U.; Hinderhofer, A.; Alonso, M. I.; Ossó, J. O.; Garriga, M.; Kytka, M.; Gerlach, A.; Schreiber, F. Uniaxial Anisotropy of Organic Thin Films Determined by Ellipsometry. *Phys. Status Solidi A* **2008**, *205*, 927–930.

(59) Kytka, M.; Gerlach, A.; Kováč, J.; Schreiber, F. Real-Time Observation of Oxidation and Photo-Oxidation of Rubrene Thin Films by Spectroscopic Ellipsometry. *Appl. Phys. Lett.* **2007**, *90*, 131911.

(60) Anger, F.; Osso, J. O.; Heinemeyer, U.; Broch, K.; Scholz, R.; Gerlach, A.; Schreiber, F. Photoluminescence Spectroscopy of Pure Pentacene, Perfluoropentacene, and Mixed Thin Films. *J. Chem. Phys.* **2012**, *136*, 054701.

(61) Heinemeyer, U.; Broch, K.; Hinderhofer, A.; Kytka, M.; Scholz, R.; Gerlach, A.; Schreiber, F. Real-Time Changes in the Optical Spectrum of Organic Semiconducting Films and Their Thickness Regimes during Growth. *Phys. Rev. Lett.* **2010**, *104*, 257401.

(62) Banerjee, R.; Novák, J.; Frank, C.; Girleannu, M.; Ersen, O.; Brinkmann, M.; Anger, F.; Lorch, C.; Dieterle, J.; Gerlach, A.; et al. Structure and Morphology of Organic Semiconductor - Nanoparticle Hybrids Prepared by Soft Deposition. *J. Phys. Chem. C* **2015**, *119*, 5225–5237.

(63) Kowarik, S.; Gerlach, A.; Leitenberger, W.; Hu, J.; Witte, G.; Wöll, C.; Pietsch, U.; Schreiber, F. Energy-Dispersive X-Ray Reflectivity and GID for Real-Time Growth Studies of Pentacene Thin Films. *Thin Solid Films* **2007**, *515*, 5606–5610.

(64) Kowarik, S.; Gerlach, A.; Sellner, S.; Cavalcanti, L.; Konovalov, O.; Schreiber, F. Real-Time X-Ray Diffraction Measurements of Structural Dynamics and Polymorphism in Diindenoperylene Growth. *Appl. Phys. A: Mater. Sci. Process.* **2009**, *95*, 233–239.

(65) Heinrich, M. A.; Pflaum, J.; Tripathi, A. K.; Frey, W.; Steigerwald, M. L.; Siegrist, T. Enantiotropic Polymorphism in Di-Indenoperylene. *J. Phys. Chem. C* **2007**, *111*, 18878–18881.

(66) Schiefer, S.; Huth, M.; Dobrinevski, A.; Nickel, B. Determination of the Crystal Structure of Substrate-Induced Pentacene Polymorphs in Fiber Structured Thin Films. *J. Am. Chem. Soc.* **2007**, *129*, 10316–10317.

(67) Campbell, R. B.; Robertson, J. M.; Trotter, J. The Crystal Structure of Hexacene, and a Revision of the Crystallographic Data for Tetracene and Pentacene. *Acta Crystallogr.* **1962**, *15*, 289–290.

(68) Hinderhofer, A.; Frank, C.; Hosokai, T.; Resta, A.; Gerlach, A.; Schreiber, F. Structure and Morphology of Coevaporated Pentacene-Perfluoropentacene Thin Films. *J. Chem. Phys.* **2011**, *134*, 104702.

(69) Wang, C.; Wang, J.; Wu, N.; Xu, M.; Yang, X.; Lu, Y.; Zang, L. Donor–Acceptor Single Cocrystal of Coronene and Perylene Diimide: Molecular Self-Assembly and Charge-Transfer Photoluminescence. *RSC Adv.* **2017**, *7*, 2382–2387.

(70) Nanova, D.; Beck, S.; Fuchs, A.; Glaser, T.; Lennartz, C.; Kowalsky, W.; Pucci, A.; Kroeger, M. Charge Transfer in Thin Films of Donor–Acceptor Complexes Studied by Infrared Spectroscopy. *Org. Electron.* **2012**, *13*, 1237–1244.

(71) Duva, G.; Beyer, P.; Scholz, R.; Belova, V.; Opitz, A.; Hinderhofer, A.; Gerlach, A.; Schreiber, F. Ground-State Charge-

Transfer Interactions in Donor:Acceptor Pairs of Organic Semiconductors—a Spectroscopic Study of Two Representative Systems. *Phys. Chem. Chem. Phys.* **2019**, *21*, 17190–17199.

(72) Sweetnam, S.; Vandewal, K.; Cho, E.; Risko, C.; Coropceanu, V.; Salleo, A.; Brédas, J. L.; McGehee, M. D. Characterizing the Polymer:Fullerene Intermolecular Interactions. *Chem. Mater.* **2016**, *28*, 1446–1452.

(73) Heinemeyer, U.; Scholz, R.; Gisslén, L.; Alonso, M. I.; Ossó, J. O.; Garriga, M.; Hinderhofer, A.; Kytka, M.; Kowarik, S.; Gerlach, A.; et al. Exciton-Phonon Coupling in Diindenoperylene Thin Films. *Phys. Rev. B: Condens. Matter Mater. Phys.* **2008**, *78*, 085210.

(74) Hinderhofer, A.; Heinemeyer, U.; Gerlach, A.; Kowarik, S.; Jacobs, R. M. J.; Sakamoto, Y.; Suzuki, T.; Schreiber, F. Optical Properties of Pentacene and Perfluoropentacene Thin Films. *J. Chem. Phys.* **2007**, *127*, 194705.

(75) Broch, K.; Heinemeyer, U.; Hinderhofer, A.; Anger, F.; Scholz, R.; Gerlach, A.; Schreiber, F. Optical Evidence for Intermolecular Coupling in Mixed Films of Pentacene and Perfluoropentacene. *Phys. Rev. B: Condens. Matter Mater. Phys.* **2011**, *83*, 245307.

(76) Sun, Y.-P.; Bunker, C. E.; Ma, B. Quantitative Studies of Ground and Excited State Charge Transfer Complexes of Fullerenes with N,N-Dimethylaniline and N,N-Diethylaniline. *J. Am. Chem. Soc.* **1994**, *116*, 9692–9699.

(77) Joseph, S.; Ravva, M. K.; Bredas, J. L. Charge-Transfer Dynamics in the Lowest Excited State of a Pentacene-Fullerene Complex: Implications for Organic Solar Cells. *J. Phys. Chem. Lett.* **2017**, *8*, 5171–5176.

(78) Gierschner, J.; Mack, H. G.; Oelkrug, D.; Waldner, I.; Rau, H. Modeling of the Optical Properties of Cofacial Chromophore Pairs: Stilbenophane. *J. Phys. Chem. A* **2004**, *108*, 257–263.

(79) Gierschner, J.; Ehni, M.; Egelhaaf, H. J.; Milián Medina, B.; Beljonne, D.; Benmansour, H.; Bazan, G. C. Solid-State Optical Properties of Linear Polyconjugated Molecules: π -Stack Contra Herringbone. *J. Chem. Phys.* **2005**, *123*, 144914.

(80) Yi, Y.; Coropceanu, V.; Brédas, J.-L. Exciton-Dissociation and Charge-Recombination Processes in Pentacene/C60 Solar Cells: Theoretical Insight into the Impact of Interface Geometry. *J. Am. Chem. Soc.* **2009**, *131*, 15777–15783.

(81) Kitaigorodsky, A. I. *Mixed Crystals*; Springer: Berlin, 1984.

(82) Aufderheide, A.; Broch, K.; Novák, J.; Hinderhofer, A.; Nervo, R.; Gerlach, A.; Banerjee, R.; Schreiber, F. Mixing-Induced Anisotropic Correlations in Molecular Crystalline Systems. *Phys. Rev. Lett.* **2012**, *109*, 156102.

(83) Martinez, C. R.; Iverson, B. L. Rethinking the Term “ π -Stacking”. *Chem. Sci.* **2012**, *3*, 2191–2201.

(84) Hunter, C. A.; Sanders, J. K. M. The Nature of π - π Interactions. *J. Am. Chem. Soc.* **1990**, *112*, 5525–5534.

(85) Lifshitz, I. M.; Slyozov, V. V. The Kinetics of Precipitation from Supersaturated Solid Solutions. *J. Phys. Chem. Solids* **1961**, *19*, 35–50.

(86) Sagui, C.; Grant, M. Theory of Nucleation and Growth during Phase Separation. *Phys. Rev. E: Stat. Phys., Plasmas, Fluids, Relat. Interdiscip. Top.* **1999**, *59*, 4175–4187.

(87) Ray, B.; Nair, P.; Alam, M. A. Annealing Dependent Performance of Organic Bulk- Heterojunction Solar Cells: A Theoretical Perspective. *Sol. Energy Mater. Sol. Cells* **2011**, *95*, 3287–3294.

(88) Zheng, C.; Bleier, D.; Jalan, I.; Pristash, S.; Penmetcha, A. R.; Hestand, N. J.; Spano, F. C.; Pierce, M. S.; Cody, J. A.; Collison, C. J. Phase Separation, Crystallinity and Monomer-Aggregate Population Control in Solution Processed Small Molecule Solar Cells. *Sol. Energy Mater. Sol. Cells* **2016**, *157*, 366–376.

(89) Opitz, A.; Ecker, B.; Wagner, J.; Hinderhofer, A.; Schreiber, F.; Manara, J.; Pflaum, J.; Brütting, W. Mixed Crystalline Films of Co-Evaporated Hydrogen- and Fluorine-Terminated Phthalocyanines and Their Application in Photovoltaic Devices. *Org. Electron.* **2009**, *10*, 1259–1267.

(90) Breuer, T.; Witte, G. Thermally Activated Intermixture in Pentacene-Perfluoropentacene Heterostructures. *J. Chem. Phys.* **2013**, *138*, 114901.

(91) Vandewal, K.; Tvingstedt, K.; Gadisa, A.; Inganäs, O.; Manca, J. V. Relating the Open-Circuit Voltage to Interface Molecular Properties of Donor:Acceptor Bulk Heterojunction Solar Cells. *Phys. Rev. B: Condens. Matter Mater. Phys.* **2010**, *81*, 125204.

(92) Salzmann, I.; Duhm, S.; Heimel, G.; Oehzelt, M.; Kniprath, R.; Johnson, R. L.; Rabe, J. P.; Koch, N. Tuning the Ionization Energy of Organic Semiconductor Films: The Role of Intramolecular Polar Bonds. *J. Am. Chem. Soc.* **2008**, *130*, 12870–12871.

(93) Duhm, S.; Heimel, G.; Salzmann, I.; Glowatzki, H.; Johnson, R. L.; Vollmer, A.; Rabe, J. P.; Koch, N. Orientation-Dependent Ionization Energies and Interface Dipoles in Ordered Molecular Assemblies. *Nat. Mater.* **2008**, *7*, 326–332.

(94) Ueno, N. Tuning Organic Band Structures with Coulomb Interactions. *Science (Washington, DC, U. S.)* **2016**, *352*, 1395–1396.

(95) Brand, C.; Meerts, W. L.; Schmitt, M. How and Why Do Transition Dipole Moment Orientations Depend on Conformer Structure? *J. Phys. Chem. A* **2011**, *115*, 9612–9619.

(96) Sun, M.; Chen, J.; Xu, H. Visualizations of Transition Dipoles, Charge Transfer, and Electron-Hole Coherence on Electronic State Transitions between Excited States for Two-Photon Absorption. *J. Chem. Phys.* **2008**, *128*, 064106.

(97) Brigeman, A. N.; Fusella, M. A.; Yan, Y.; Purdum, G. E.; Loo, Y. L.; Rand, B. P.; Giebink, N. C. Revealing the Full Charge Transfer State Absorption Spectrum of Organic Solar Cells. *Adv. Energy Mater.* **2016**, *6*, 1601001.

(98) Endres, R. G.; Fong, C. Y.; Yang, L. H.; Witte, G.; Wöll, C. Structural and Electronic Properties of Pentacene Molecule and Molecular Pentacene Solid. *Comput. Mater. Sci.* **2004**, *29*, 362–370.

(99) Soos, Z. G.; Hennessy, M. H.; Wen, G. Frenkel and Charge Transfer States of Conjugated Polymers and Molecules. *Chem. Phys.* **1998**, *227*, 19–32.

(100) Hennessy, M. H.; Soos, Z. G.; Pascal, R. A.; Girlando, A. Vibronic Structure of PTCDA Stacks: The Exciton-Phonon-Charge-Transfer Dimer. *Chem. Phys.* **1999**, *245*, 199–212.

(101) Gisslén, L.; Scholz, R. Crystallochromy of Perylene Pigments: Interference between Frenkel Excitons and Charge-Transfer States. *Phys. Rev. B: Condens. Matter Mater. Phys.* **2009**, *80*, 115309.

(102) Hestand, N. J.; Yamagata, H.; Xu, B.; Sun, D.; Zhong, Y.; Harutyunyan, A. R.; Chen, G.; Dai, H. L.; Rao, Y.; Spano, F. C. Polarized Absorption in Crystalline Pentacene: Theory vs Experiment. *J. Phys. Chem. C* **2015**, *119*, 22137–22147.